physica status solidi rrl
www.pss-rapid.com

Covalent Mixing in the 2D Ferromagnet $CrSiTe_3$ Evidenced by Magnetic X-Ray Circular Dichroism

Barat Achinuq, Ryuji Fujita, Wei Xia, Yanfeng Guo, Peter Bencok, Gerrit van der Laan, and Thorsten Hesjedal**

The low-temperature electronic structure of the van der Waals ferromagnet $CrSiTe_3$ is investigated. This ferromagnetic semiconductor has a magnetic bulk transition temperature of 33 K, which can reach up to 80 K in single- and few-layer flakes. X-ray absorption spectroscopy (XAS) and X-ray magnetic circular dichroism (XMCD) measurements, carried out at the Cr $L_{2,3}$ and Te M_5 edges in vacuo-cleaved single crystals, give strong evidence for hybridization-mediated superexchange between the Cr atoms. The observed chemical shift in the XAS, as well as the comparison of XMCD with the calculated Cr $L_{2,3}$ multiplet spectra, confirms a strong covalent bond between the Cr $3d(e_g)$ and Te $5p$ states. Application of the XMCD sum rules gives a nonvanishing orbital moment, supporting a partial occupation of the e_g states, apart from t_{2g}. Also, the presence of a nonzero XMCD signal at the Te M_5 edge confirms a Te $5p$ spin polarization due to mixing with the Cr e_g bonding states. The results strongly suggest that superexchange, instead of the previously suggested single-ion anisotropy, is responsible for the low-temperature ferromagnetic ordering of 2D materials such as $CrSiTe_3$ and $CrGeTe_3$. This demonstrates the interplay between electron correlation and ferromagnetism in insulating 2D materials.

1. Introduction

2D van der Waals materials[1] and their heterostructures have been the focus of materials research ever since the field started off with the discovery of grapheme.[2] Among the 2D materials, magnetically ordered films have caught the attention of the magnetism community as they promise the possibility of further device scaling. Despite being in principle "forbidden" at finite temperatures due to fluctuations (Mermin–Wagner theorem[3]), long-range magnetic order can occur in 2D systems when taking into account magnetocrystalline anisotropy. The breaking of spin rotational invariance can be described by several mechanisms, such as dipolar interactions, single-ion anisotropy, and/or anisotropy of the exchange interaction.[4] Earlier theoretical studies of layered Mn- and Cr-based semiconducting trichalcogenide monolayers, which predicted the crystallographically very similar compounds $CrSiTe_3$ to be antiferromagnetically and $CrGeTe_3$ to be ferromagnetically ordered (with a Curie temperature of 106 K), have sparked intense experimental studies of these and related compounds.[5] It is important to note that despite their close similarities such as their ferromagnetic bulk properties (in contrast to the prediction of $CrSiTe_3$ being an antiferromagnet),[6–8] the very different magnetic properties of $CrSiTe_3$ compared with $CrGeTe_3$ monolayers are due to minute differences in their second- and third-nearest neighbor exchange interactions,[5] the larger van der Waals (vdW) gap, and the smaller Cr–Cr distance.[9] Also, while the interlayer coupling in $CrSiTe_3$ is antiferromagnetic, the intralayer coupling is ferromagnetic, and the overall properties of the material therefore strongly depend on the c-axis lattice constant.[5] The thickness dependence of the magnetic properties of $CrSiTe_3$, down to single- and few-

B. Achinuq[+], R. Fujita, T. Hesjedal
Department of Physics
Clarendon Laboratory
University of Oxford
Oxford OX1 3PU, UK
E-mail: thorsten.hesjedal@physics.ox.ac.uk

The ORCID identification number(s) for the author(s) of this article can be found under https://doi.org/10.1002/pssr.202100566.

[+]Dr. B. Achinuq formerly known as Dr. Balati Kuerbanjiang

DOI: 10.1002/pssr.202100566

W. Xia, Y. Guo
School of Physical Science and Technology
ShanghaiTech University
Shanghai 201210, China

W. Xia, Y. Guo
ShanghaiTech Laboratory for Topological Physics
ShanghaiTech University
Shanghai 201210, China

P. Bencok, G. van der Laan
Diamond Light Source
Harwell Science and Innovation Campus
Didcot, Oxfordshire OX11 0DE, UK
E-mail: gerrit.vanderlaan@diamond.ac.uk

monolayer flakes, has been investigated via Hall measurements.[10] From the observed change in resistivity at 80−120 K, the Curie temperature of those flakes was estimated to be ≈80 K.[10] This remarkable increase from the bulk value of 33 K[6,7,11] is in stark contrast to the behavior of other 2D ferromagnets and has been proposed to stem from the increased intralayer superexchange interaction via Te in the few-layer limit.[9,12] Recently, in the ultrathin layer limit, the thickness-dependent magnetic transition from 3D (Heisenberg) to 2D Ising behavior has been observed for a $CrSiTe_3$ thickness of ≈7 nm, which goes hand in hand with a drop in Curie temperature from 33 to 17 K.[13] This behavior is often tied to the strong dependence of the electronic structure on the reduced dimensionality in the ultrathin layer limit, as it has been experimentally observed for CrI_3.[1]

$CrSiTe_3$ crystallizes in the space group $R\bar{3}$. Its reported effective moment $\mu_{\text{eff}} = 3.88(2)\ \mu_B$ $(H\|c)$ is in good agreement with the moment expected for Cr^{3+},[7] and so is the saturation moment at 2 K of 3.08 μ_B (compared with 3 μ_B for Cr^{3+} with three unpaired spins). $CrSiTe_3$ shows almost no hysteresis with very small remanent magnetization of 0.001 μ_B $(H\|c)$.[7] From a detailed analysis of the critical behavior of the magnetic phase transition, it was concluded that $CrSiTe_3$ can be described with a 2D Ising model coupled with long-range interaction.[14] The bulk T_C is also very sensitive to the applied pressure, and an increase from 33 to 138 K has been reported, also changing the soft magnetic normal behavior to a hard magnetic one.[15] Therefore, the exploration of the mechanism behind the magnetic ordering of 2D $CrSiTe_3$ is an important yet challenging task.

In an ionic picture, the oxidation state of Cr in $CrSiTe_3$ and $CrGeTe_3$ is expected to be +3 with an electronic configuration $3d^3$. In an octahedral environment, these d levels split into a higher energy e_g doublet and a lower energy t_{2g} triplet. Thus, Cr^{3+} ions have $S = 3/2$, with three unpaired electrons in the half-filled t_{2g} manifold, in compliance with the first Hund rule. This is consistent with the observed saturation magnetization of bulk $CrSiTe_3$ that yields a magnetic moment of ≈3 μ_B/Cr.[7] The lack of orbital degeneracy of the orbital singlet state $^4A_2$ with $L = 0$ leads to a vanishing magnetocrystalline anisotropy energy $E_{\text{MCA}} \propto \lambda\langle L\rangle \cdot \langle S\rangle$, where λ is the $3d$ spin−orbit interaction parameter. The slightly distorted octahedral symmetry, with its bond angles deviating from 90°, has point group symmetry D_{3d}. Under lower symmetry, the t_{2g} state splits into $a_{1g} + e_g^{\pi}$ and the e_g state is relabeled as e_g^{σ}. Long-range ferromagnetism in $CrSiTe_3$ arises from the superexchange between the neighboring e_g^{π} and e_g^{σ} states, consistent with the Goodenough−Kanamuri rule.[16,17] This model is supported by angular-resolved photoelectron emission spectroscopy (ARPES) results and density functional theory (DFT) + dynamical mean-field theory (DMFT) calculations on $CrSiTe_3$.[18] In magnetic insulators dominated by superexchange, as realized in many transition metal oxide and chalcogenide materials, the superexchange between the spins on neighboring metal sites depends on the electron hopping (charge transfer) between the metal $3d$ and neighboring ligand p states.[19] Above the Curie temperature, the Coulomb repulsion drives the system into a charge transfer insulator phase.[18]

Here we report the X-ray absorption spectroscopy (XAS) and X-ray magnetic circular dichroism (XMCD) of the low-temperature ferromagnetic phase of $CrSiTe_3$. These element-specific techniques offer the most direct way to determine the local electronic and magnetic structure of $3d$ transition metal atoms due to their valence, site, and symmetry selectivity.[20–23] Some recent reports in the literature have claimed that their XMCD measurements on $CrSiTe_3$[24] and $CrGeTe_3$[25] confirm the single-ion anisotropy of the octahedrally distorted Cr^{3+} to be responsible for the long-range ferromagnetic ordering. In contrast, here we show that, while single-ion anisotropy may play a role, the main contribution arises from the hybridization-mediated superexchange between the Cr atoms. We show that the calculated Cr $L_{2,3}$ multiplet spectrum in the presence of crystal-field and spin−orbit interaction provides unique information regarding the hybridized ground state.[20] The XMCD sum rule analysis[26,27] establishes a nonvanishing orbital moment, indicating a partial occupation of $3d(e_g)$ states. The observation of XMCD at the Te M_5 edge confirms a Te $5p$ spin polarization aligned with the Cr $3d$ moment.

2. Experimental Section

2.1. Structural and Magnetic Characterization

$CrSiTe_3$ single crystals were grown using a self-flux method, as described in detail in the study by Suo et al.[28] The resulting plate-like crystals, which measure ≈8 mm across, were characterized by room-temperature X-ray diffraction (XRD) using a Mo Kα ($\lambda = 0.7107$ Å) source in SuperNova single-crystal XRD system. $CrSiTe_3$ crystallizes in the $R\bar{3}$ space group (**Figure 1**a–c), consistent with the single-crystal XRD data shown in Figure 1d, from which we determined the following lattice parameters: $a = 6.7699$ Å, $b = 6.7699$ Å, and $c = 20.6825$ Å ($\alpha = \beta = 90°$ and $\gamma = 120°$), in agreement with the study by Ouvrard et al.[29] The layered structure of $CrSiTe_3$ can be seen in Figure 1b, where the ≈3.5 Å-thick Cr−Si−Te quintuple layers with their Te terminations are separated by a ≈3.3 Å vdW gap.[7,30] The stacking sequence of the Cr−Si−Te quintuple layers in the unit cell was A−B−C. The crystal orientation of the vdW cleavage planes was normal to the c-axis.

The temperature-dependent magnetic properties of the sample were studied using bulk-sensitive superconducting quantum interference device (SQUID) magnetometry (Quantum Design 7T MPMS SQUID VSM). From the temperature dependence of magnetization, shown in **Figure 2**, a transition temperature of 32.8 K was estimated (defined as the minimum of the derivative; shown as an inset), consistent with previous studies.[6,7,11] In agreement with earlier reports,[7] $CrSiTe_3$ showed no hysteretic behavior and a negligible remanent magnetization. Detailed magnetic data on our sample can be found in the study by Zhang et al.[18]

2.2. XAS and Magnetic Circular Dichroism

XAS and XMCD measurements were carried out using the electromagnet end-station ELMA on beamline I10 at the Diamond Light Source, UK. The sample was cleaved in ultrahigh vacuum in the magnet chamber. For this purpose, a small ceramic cleaving post was glued to the single crystal, which could be hit in a

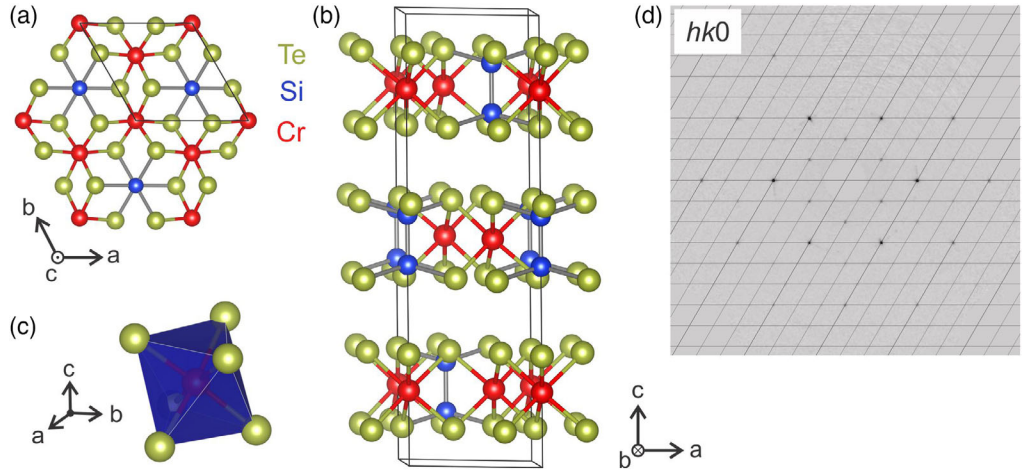

Figure 1. Crystal structure of $CrSiTe_3$ viewed along the a) the *c*-axis and b) normal to the *ac*-plane. The $CrSiTe_3$ monolayers are terminated by Te layers, which form a van der Waals gap. c) The coordination octahedron shows the Cr ion in the center of six Te ions. d) Single-crystal diffraction pattern showing the reciprocal space points in the (*hk*0) plane at room temperature. A dashed grid in units of reciprocal lattice constants is shown for convenience.

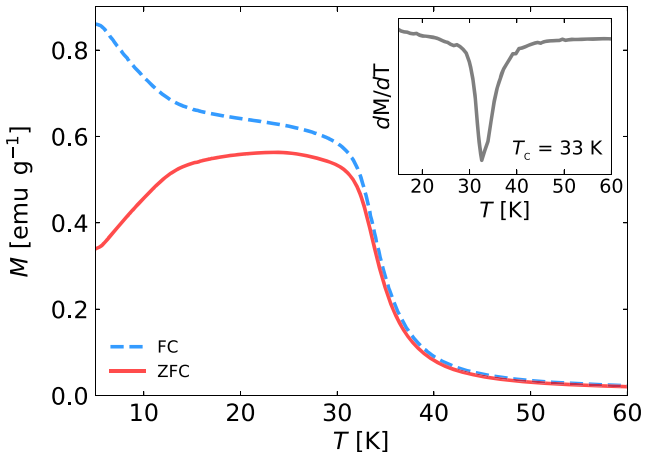

Figure 2. Temperature dependence of the magnetization after zero field cooling (ZFC) and field cooling (FC) in an applied field of 1 T. The measurements were performed in an applied out-of-plane field of 10 mT. The inset shows the temperature derivative of the magnetization, revealing a T_C (taken as the minimum) of 33 K.

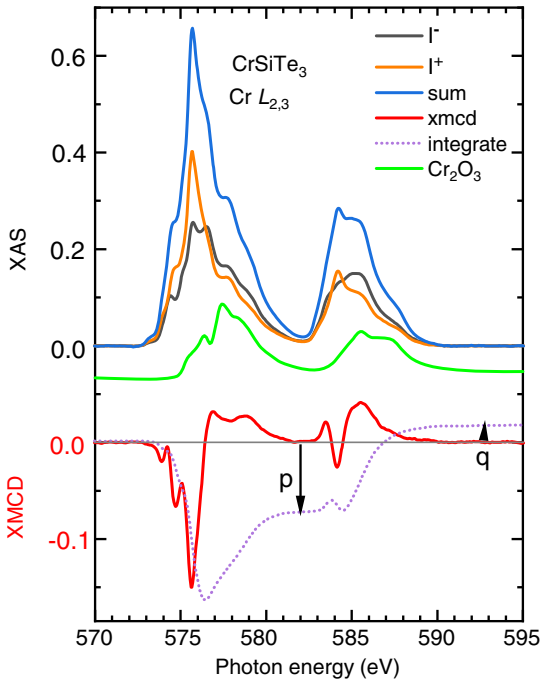

Figure 3. Experimental Cr $L_{2,3}$ XAS and XMCD of $CrSiTe_3$ at 10 K and 1.4 T. Upper part: XAS for I^+ (orange curve), I^- (black curve), sum spectrum ($I^- + I^+$) (blue curve), and the Cr_2O_3 reference (green curve). Lower part: XMCD spectrum ($I^- - I^+$) (red curve), shown on a 2× expanded scale compared with XAS, together with its integrate (dotted curve). The arrows with labels *p* and *q* indicate the integrated intensities over the L_3 and $L_{2,3}$ edges, respectively.

controlled way using the sample transfer tool. Spectra were measured with 100% left- (LCP) and right-circularly polarized (RCP) light and positive and negative fields $H = \pm 1.4$ T using total-electron yield detection, which probed the top 3–5 nm of the sample,[23] at a temperature of 10 K. The field was along the X-ray beam, at normal incidence to the sample surface. Adhering to the sign convention,[23] we took the spectra $I^- = \frac{1}{2}[I_{\mathrm{LCP}}(H) + I_{\mathrm{RCP}}(-H)]$, $I^+ = \frac{1}{2}[I_{\mathrm{RCP}}(H) + I_{\mathrm{LCP}}(-H)]$, $I_{\mathrm{sum}} = I^- + I^+$, and $I_{\mathrm{xmcd}} = I^- - I^+$. A reference sample of Cr_2O_3 was used to calibrate the photon energy, as well as to verify whether the measured $CrSiTe_3$ spectra showed a fraction corresponding to a surface oxide.

The element-specific spin and orbital magnetic moments were obtained from the integrated intensities of the dichroic spectra using the sum rule analysis.[31] **Figure 3** shows the integrate of the XMCD spectra, with *p* and *q* the integrated intensities over the L_3 and $L_{2,3}$ edges, respectively. From the values of *p* and *q*, and using the integrated intensity *r* over the $L_{2,3}$ edge of the sum spectrum as the normalization factor accounting for the number of *d* holes $n_h = (10 - n_d)$, we obtained the spin and

orbital moments per Cr atom as follows: $m_L = -\langle L_z \rangle = -(4/3)qn_h/r$ and $m_S = -\langle 2S_{eff,z} \rangle = -(6p - 4q)Cn_h/r$.[23] For the lighter $3d$ metals, the spin sum rule contains the correction factor C, which is equal to 2.0 for Cr, to rectify for the large overlap of $2p_{3/2}$ and $2p_{1/2}$ multiplet structures.[32] As suggested by the Cr_2O_3 contribution at the high-energy side, we assumed that ≈10% of the XAS intensity of $CrSiTe_3$ came from the oxide and corrected the value of r accordingly.

2.3. Multiplet calculations

Atomic multiplet calculations were performed to compute the Cr $L_{2,3}$ XAS and XMCD spectra for the electric–dipole transitions, $3d^n \rightarrow 2p^5 3d^{n+1}$, with the spin–orbit and electrostatic interactions treated on an equal footing.[33,34] The wave functions of the initial- and final-state configurations were calculated in intermediate coupling using Cowan's atomic Hartree–Fock (HF) code with relativistic corrections.[20,35] The atomic electrostatic interactions included the $3d$–$3d$ and $2p$–$3d$ Coulomb and exchange interactions, which were reduced to 80% and 75%, respectively, of their atomic HF value to account for intraatomic screening.[33] Hybridization was included by mixing the Cr $3d^3$ and $3d^4\underline{L}$ wave functions, where $\underline{L}$ represented a hole on the neighboring atoms in states of appropriate symmetry. For $CrSiTe_3$, the charge transfer energies in the initial and final state were taken as $E(3d^4\underline{L}) - E(3d^3) = -1$ eV and $E(2p^5 3d^5\underline{L}) - E(2p^5 3d^4) = -3$ eV, respectively, where E stands for the average energy of the configuration in the parentheses. The hybridization parameter was taken as $T = \langle \Psi(d^3)|H|\Psi(d^4\underline{L})\rangle = 1.7$ eV. The Cr ions were located at the center of a slightly distorted octahedron of Te atoms.[7] An octahedral crystal field of $10Dq = 1.8$ eV was included in the calculation. The computed Cr L_3 (L_2) line spectra were convoluted by a Lorentzian with a half width of $\Gamma = 0.2$ eV (0.4 eV) for intrinsic lifetime broadening and a Gaussian with a standard deviation of $\sigma = 0.15$ eV for instrumental broadening.

3. Results and Discussion

The XAS and XMCD of $CrSiTe_3$ at the Cr $L_{2,3}$ edge measured at 10 K and 1.4 T are shown in Figure 3. As expected, no XMCD was observed above the Curie temperature (not shown). Compared with the Cr_2O_3 (Cr^{3+}, d^3) reference sample (green curve), the Cr $L_{2,3}$ edge of $CrSiTe_3$ is shifted to lower photon energy. Qualitatively, this chemical shift implies a higher d-electron count in $CrSiTe_3$ as compared with Cr_2O_3.[21] It appears that at the high-energy side of both the L_3 and L_2 edges in the XAS, there is a small contribution of chromium oxide present, estimated to ≈10%. Assuming that this oxide is antiferromagnetic, it will not give an XMCD signal.[36] Most likely, this oxide contribution originates from the edges of the cleaved crystal, as the X-ray beam spot (≈1 mm horizontally) is on the order of the sample size (≈1 × 2 mm^2; thickness: ≈2–3 μm).

Much information can be gained by comparison of the measured spectra with atomic multiplet calculations. Calculated spectra for the ionic configurations Cr d^3 and Cr d^4 with different values of the octahedral crystal field parameter $10Dq$ can be found in the study by van der Laan.[20] It becomes clear that none of the calculated spectra for a pure ionic configuration gives a particularly good fit to the $CrSiTe_3$ spectra. To obtain a better agreement between the measured and calculated spectra requires treating the ground state of Cr as a hybridized state with ≈50% d^3 and 50% $d^4\underline{L}$ character, corresponding to a d electron count of $n_d \approx 3.5$ (for details and parameter values, see Section 2.3). This reproduces very well the measured XMCD spectrum (**Figure 4**). The hybridization with the $d^4\underline{L}$ state also leads to lowering in photon energy by ≈1.5 eV compared with the ionic d^3 configuration. This chemical shift has also been reported for other Cr atoms in a tellurium octahedral environment with $n_d > 3$.[32,37–39]

It is interesting to compare the spectral shape of the XMCD with that of related compounds. The XMCD spectrum of $CrSiTe_3$ resembles that of the structurally similar $CrGeTe_3$ ($T_C \approx 63$ K)[39] and CrI_3 ($T_C \approx 45$ K)[40] (see Figure 4). However, the XMCD line shape is very different compared with some of the other $CrTe_6$ octahedra-hosting compounds, such as Cr-doped Sb_2Te_3[38]; the latter shows a similar XMCD spectral shape as Cr-doped Bi_2Se_3.[32,37] In both magnetically doped topological insulators, Cr has 30% d^3 and 70% $d^4\underline{L}$ character ($n_d \approx 3.7$). Compared with Cr:Sb_2Te_3, the XMCD spectra of $CrSiTe_3$, $CrGeTe_3$, and CrI_3 show a much more pronounced multiplet structure with sharp peaks. The energy separation between the two main negative peaks at the L_3 edge is significantly smaller in $CrSiTe_3$ (0.95 eV) compared with $CrGeTe_3$ and CrI_3 (1.1 eV). This does not seem to be related to the vdW interlayer gap in the various materials. The vdW spacing

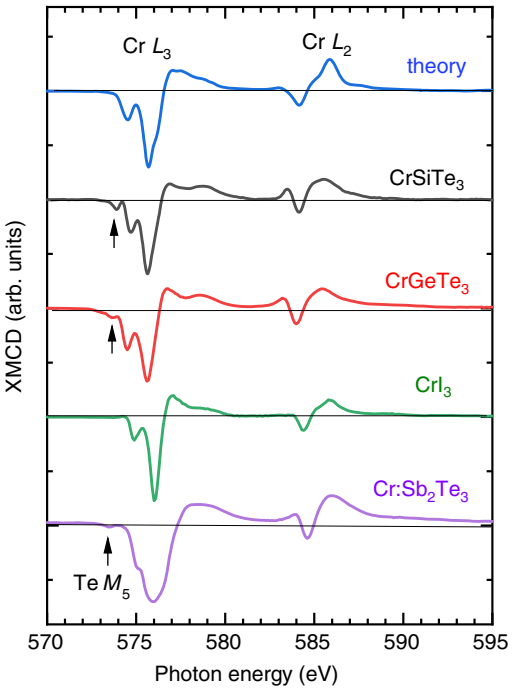

Figure 4. Comparison of Cr $L_{2,3}$ XMCD spectra for $CrSiTe_3$ (this work), $CrGeTe_3$[39] CrI_3,[40] $Cr_{0.32}Sb_{1.68}Te_3$,[38] and the theoretical multiplet spectrum [this work]. The black arrow at ≈573.8 eV marks the position of the Te M_5 peak. The spectra are normalized to maximum peak intensity and vertically shifted for clarity.

of $CrGeTe_3$ is 3.39 Å,[8,41] which is slightly larger than the value of 3.3 Å of $CrSiTe_3$. The vdW spacing of CrI_3 is reported to be even as large as 3.488 Å.[42]

For the measured Cr $L_{2,3}$ spectra of $CrSiTe_3$ at a temperature of 10 K, the application of the orbital sum rule (for equations, see Section 2.2) using $n_d = 3.5$ gives an orbital moment of $m_L = (-0.055 \pm 0.05)\mu_B$/Cr. In comparison, $m_L = -0.045$ (out of plane) and -0.052 (in plane) for $CrGeTe_3$ and m_L is -0.051 for CrI_3 at 20 K.[43] Application of the spin sum rule gives an effective spin moment $m_S = (2.86 \pm 0.25)\ \mu_B$/Cr (i.e., $0.82\mu_B$ per 3*d* electron). When Cr reduces its symmetry from a pure t_{2g}^3 ($^4A_2$) configuration in octahedral symmetry to D_{3d}, or when e_g is partially occupied, the effective spin moment contains a finite contribution of the magnetic dipole term $\langle T_z \rangle$, which can reach up to ±10% of the total spin moment.[44] Thus, the measured spin moment is close to $m_S \approx 3\mu_B$/Cr that was reported using conventional magnetization measurements.[7]

From the calculated spectrum (also shown in Figure 4), we find $m_L = -0.022\ \mu_B$/Cr and $m_S = 2.81\ \mu_B$/Cr (i.e., 0.80 μ_B per 3*d* electron), which is a very similar result as from the experiment. The fact that the full spin polarization of 3.5 μ_B/Cr is not reached is due to the spin–orbital-coupled nature of the multideterminant wave function for less-than-half-filled configuration where the spin and orbital moments form an entangled state.[34,35]

According to the third Hund's rule, the spin and orbital moments for the less-than-half-filled Cr band are aligned antiparallel. Indeed, from the sum rule analysis, we find $m_L/m_S = -0.019$. Furthermore, this excludes that we are dealing with an ionic configuration Cr^{3+} t_{2g}^3 that has $m_L = 0$. This is a further indication of the partial occupation of the e_g state due to the hybridization with the Te 5*p* states.

Similar to $CrGeTe_3$,[39] the *d*-count of $n_d \approx 3.5$ indicates a Cr ionic configuration with three electrons in the t_{2g} state and ≈0.5 electron in the e_g state, with parallel spins according to the first Hund's rule. While the overlap of t_{2g} with the Te 5*p* is small, that of the e_g state is large, resulting in covalent bonding. This hybridization (mixing) leads to unoccupied states in the otherwise-filled Te 5*p* band, giving rise to the appearance of a nonzero XMCD signal at the Te M_5 edge. The size of Te M_5 XMCD is expected to scale with the number of holes in the Te 5*p* band and hence the hybridization.

However, in Cr-based materials, it is challenging to observe the Te M_5 edge as its energy position is close to that of the Cr L_3 edge, while its cross section is much smaller.[38] Nonetheless, in both the XAS and XMCD spectra, we find a small peak at 573.8 eV (black arrows in Figure 4), which agrees well with the energy position at which the Te M_5 edge is expected (see Figure S9c in the Supplementary Material of the study by Figueroa et al.[45]). The absence of such a tellurium feature in the XAS/XMCD of CrI_3 as well as in the multiplet calculation for the Cr-mixed configuration (Figure 4) supports that the peak observed at 573.8 eV originates indeed from the Te M_5 edge. The Te M_5 exhibits a negative XMCD signal, with the same sign as the Cr L_3 edge (Figure 4). As the azimuthal quantum numbers for the orbitals in these two electric–dipole transitions are opposite (Te $3d \rightarrow 5p$ and Cr $2p \rightarrow 3d$, respectively), the moments of less-than-half-filled Cr and the nearly filled Te bands are aligned antiparallel, as should be the case for electronic mixing.

4. Conclusion

In summary, we performed XAS and XMCD on freshly cleaved $CrSiTe_3$ crystals below the magnetic ordering temperature. The experimental Cr $L_{2,3}$ XMCD, present below T_C, shows good agreement with the calculated spectrum for a hybridized ground state. Our experimental results suggest that the hybridization between the Cr and Te states is responsible for the magnetic anisotropy that lies behind the 2D magnetic behavior of $CrSiTe_3$. The evidence for covalent mixing arises from the comparison of the measured XMCD with multiplet calculations, indicating ≈3.5 electrons at the Cr 3*d* side, a large chemical shift to lower photon energy, and the observation of an XMCD signal at the Te M_5 edge that demonstrates a 5*p* spin polarization on the neighboring Te atoms. The orbital-to-spin moment ratio $m_L/m_S = -0.019$ for Cr 3*d*, extracted from the sum rules, provides additional support for the presence of e_g bonding orbitals that hybridize with the Te 5*p* states, enabling superexchange that gives long-range ferromagnetic order. Comparison with other 2D magnetic vdW materials such as $CrGeTe_3$ and CrI_3, which show similar although not quite identical XMCD spectra, suggests that the superexchange model provides a general picture for such types of 2D materials.

Acknowledgements

Beamtime awarded on the electromagnet end station on I10 at the Diamond Light Source under proposal MM28727-2 is acknowledged. Y.F.G. acknowledges the open projects from State Key Laboratory of Surface Physics and Department of Physics, Fudan University (grant no. KF2020_09), and National Laboratory of Solid State Microstructures, Nanjing University (grant no. M34015). B.A. and T.H. acknowledge funding from the Engineering and Physical Sciences Research Council (EP/N032128/1) and thank RCaH for access to the scanning electron microscope/energy dispersive spectroscopy (SEM/EDS) facility.

Conflict of Interest

The authors declare no conflict of interest.

Data Availability Statement

The data that support the findings of this study are available from the corresponding author upon reasonable request.

Keywords

magnetic 2D materials, magnetic spectroscopy, X-ray techniques

Received: November 8, 2021
Revised: December 10, 2021
Published online: December 30, 2021

[1] B. Huang, G. Clark, E. Navarro-Moratalla, D. R. Klein, R. Cheng, K. L. Seyler, D. Zhong, E. Schmidgall, M. A. McGuire, D. H. Cobden, W. Yao, D. Xiao, P. Jarillo-Herrero, X. Xu, *Nature* **2017**, *546*, 270.
[2] A. K. Geim, I. V. Grigorieva, *Nature* **2013**, *499*, 419.
[3] N. D. Mermin, H. Wagner, *Phys. Rev. Lett.* **1966**, *17*, 1133.
[4] J. L. Lado, J. Fernández-Rossier, *2D Mater.* **2017**, *4*, 035002.
[5] N. Sivadas, M. W. Daniels, R. H. Swendsen, S. Okamoto, D. Xiao, *Phys. Rev. B* **2015**, *91*, 235425.
[6] V. Carteaux, F. Moussa, M. Spiesser, *Europhys. Lett.* **1995**, *29*, 251.
[7] L. D. Casto, A. J. Clune, M. O. Yokosuk, J. L. Musfeldt, T. J. Williams, H. L. Zhuang, M.-W. Lin, K. Xiao, R. G. Hennig, B. C. Sales, J.-Q. Yan, D. Mandrus, *APL Mater.* **2015**, *3*, 041515.
[8] V. Carteaux, D. Brunet, G. Ouvrard, G. Andre, *J. Phys.: Condens. Matter* **1995**, *7*, 69.
[9] X. Jiang, Q. Liu, J. Xing, N. Liu, Y. Guo, Z. Liu, J. Zhao, *Appl. Phys. Rev.* **2021**, *8*, 031305.
[10] M.-W. Lin, H. L. Zhuang, J. Yan, T. Z. Ward, A. A. Puretzky, C. M. Rouleau, Z. Gai, L. Liang, V. Meunier, B. G. Sumpter, P. Ganesh, P. R. C. Kent, D. B. Geohegan, D. G. Mandrus, K. Xiao, *J. Mater. Chem. C* **2016**, *4*, 315.
[11] V. Carteaux, G. Ouvrard, J. C. Grenier, Y. Laligant, *J. Magn. Magn. Mater.* **1991**, *94*, 127.
[12] M. S. Baranava, D. C. Hvazdouski, V. A. Skachkova, V. R. Stempitsky, A. L. Danilyuk, *Mater. Today: Proc.* **2020**, *20*, 342.
[13] C. Zhang, L. Wang, Y. Gu, X. Zhang, L.-L. Huang, Y. Fu, C. Liu, J. Lin, X. Zou, H. Su, J.-W. Mei, J.-F. Dai, arXiv:2111.05495 **2021**.
[14] B. Liu, Y. Zou, L. Zhang, S. Zhou, Z. Wang, W. Wang, Z. Qu, Y. Zhang, *Sci. Rep.* **2016**, *6*, 33873.
[15] C. Zhang, Y. Gu, L. Wang, L.-L. Huang, Y. Fu, C. Liu, S. Wang, H. Su, J.-W. Mei, X. Zou, J.-F. Dai, *Nano Lett.* **2021**, *21*, 7946.
[16] J. Kanamori, *J. Phys. Chem. Solids* **1959**, *10*, 87.
[17] H. Weihe, H. U. Güdel, *Inorg. Chem.* **1997**, *36*, 3632.
[18] J. Zhang, X. Cai, W. Xia, A. Liang, J. Huang, C. Wang, L. Yang, H. Yuan, Y. Chen, S. Zhang, Y. Guo, Z. Liu, G. Li, *Phys. Rev. Lett.* **2019**, *123*, 047203.
[19] D. I. Khomski, *Transition Metal*, Cambridge University Press, Cambridge **2014**.
[20] G. van der Laan, B. T. Thole, *Phys. Rev. B* **1991**, *43*, 13401.
[21] G. van der Laan, I. W. Kirkman, *J. Phys.: Condens. Matter* **1992**, *4*, 4189.
[22] G. van der Laan, *J. Phys. Conf. Ser.* **2013**, *430*, 012127.
[23] G. van der Laan, A. I. Figueroa, *Coord. Chem. Rev.* **2014**, *277–278*, 95.
[24] W. Niu, X. Zhang, W. Wang, J. Sun, Y. Xu, W. Liu, Y. Pu, *Appl. Phys. Lett.* **2021**, *119*, 172402.
[25] M. Suzuki, B. Gao, G. Shibata, S. Sakamoto, Y. Nonaka, K. Ikeda, Z. Chi, Y.-X. Wan, T. Takeda, T. Koide, A. Tanaka, M. Kobayashi, S.-W. Cheong, A. Fujimori, arXiv:2109.05715v1 **2021**.
[26] B. T. Thole, P. Carra, F. Sette, G. van der Laan, *Phys. Rev. Lett.* **1992**, *68*, 1943.
[27] P. Carra, B. T. Thole, M. Altarelli, X. Wang, *Phys. Rev. Lett.* **1993**, *70*, 694.
[28] P. Suo, W. Xia, W. Zhang, X. Zhu, J. Fu, X. Lin, Z. Jin, W. Liu, Y. Guo, G. Ma, *Laser Photonics Rev.* **2020**, 14, *7*, 2000025.
[29] G. Ouvrard, E. Sandre, R. Brec, *J. Solid State Chem.* **1988**, *73*, 27.
[30] A. Milosavljević, A. Šolajić, J. Pešić, Y. Liu, C. Petrovic, N. Lazarević, Z. V. Popović, *Phys. Rev. B* **2018**, *98*, 104306.
[31] G. van der Laan, *Phys. Rev. B* **1998**, *57*, 112.
[32] A. I. Figueroa, G. van der Laan, L. J. Collins-McIntyre, S.-L. Zhang, A. A. Baker, S. E. Harrison, P. Schönherr, G. Cibin, T. Hesjedal, *Phys. Rev. B* **2014**, *90*, 134402.
[33] B. T. Thole, G. van der Laan, J. C. Fuggle, G. A. Sawatzky, R. C. Karnatak, J. M. Esteva, *Phys. Rev. B* **1985**, *32*, 5107.
[34] G. van der Laan, *Lect. Notes Phys.* **2006**, *697*, 143.
[35] R. D. Cowan, *The Theory of Atomic Structure and Spectra*, University of California Press, Berkeley, **1992**.
[36] K. Toyoki, Y. Shiratsuchi, T. Nakamura, C. Mitsumata, S. Harimoto, Y. Takechi, T. Nishimura, H. Nomura, R. Nakatani, *Appl. Phys. Express* **2014**, *7*, 114201.
[37] A. A. Baker, A. I. Figueroa, K. Kummer, L. J. Collins-McIntyre, T. Hesjedal, G. van der Laan, *Phys. Rev. B* **2015**, *92*, 094420.
[38] L. B. Duffy, A. I. Figueroa, L. Gładczuk, N.-J. Steinke, K. Kummer, G. van der Laan, T. Hesjedal, *Phys. Rev. B* **2017**, *95*, 224422.
[39] M. D. Watson, I. Markovic, F. Mazzola, A. Rajan, E. A. Morales, D. M. Burn, T. Hesjedal, G. van der Laan, S. Mukherjee, T. K. Kim, C. Bigi, I. Vobornik, M. C. Hatnean, G. Balakrishnan, P. D. C. King, *Phys. Rev. B* **2020**, *101*, 205125.
[40] A. Frisk, L. B. Duffy, S. Zhang, G. van der Laan, T. Hesjedal, *Mater. Lett.* **2018**, *232*, 5.
[41] Y. F. Li, W. Wang, W. Guo, C. Y. Gu, H. Y. Sun, L. He, J. Zhou, Z. B. Gu, Y. F. Nie, X. Q. Pan, *Phys. Rev. B* **2018**, *98*, 125127.
[42] M. A. McGuire, H. Dixit, V. R. Cooper, B. C. Sales, *Chem. Mater.* **2015**, *27*, 612.
[43] D.-H. Kim, K. Kim, K.-T. Ko, J.-H. Seo, J. S. Kim, T.-H. Jang, Y. Kim, J.-Y. Kim, S.-W. Cheong, J.-H. Park, *Phys. Rev. Lett.* **2019**, *122*, 207201.
[44] J. Stöhr, H. König, *Phys. Rev. Lett.* **1995**, *75*, 3748.
[45] A. I. Figueroa, F. Bonell, M. G. Cuxart, M. Valvidares, P. Gargiani, G. van der Laan, A. Mugarza, S. O. Valenzuela, *Phys. Rev. Lett.* **2020**, *125*, 226801.